

MASS AND COLOR DEPENDENCE OF THE THREE-POINT CORRELATION FUNCTION OF GALAXIES IN THE LOCAL UNIVERSE

HONG GUO^{1,2}, CHENG LI¹, Y. P. JING³, GERHARD BÖRNER⁴

Draft version March 12, 2019

Abstract

We measure the three-point correlation function (3PCF) of the SDSS DR7 main sample galaxies in both redshift and projected spaces on scales up to $40 h^{-1}\text{Mpc}$. The dependence of the 3PCF on stellar mass and color is explored in different scales and triangle shapes. We find a weak but significant stellar mass dependence. More massive galaxies generally have higher amplitudes of the 3PCF, but lower amplitudes of the reduced 3PCF. The reduced 3PCF in both redshift and projected spaces only has mild shape dependence on small scales ($< 2 h^{-1}\text{Mpc}$), regardless of stellar mass and color. The shape dependence of the reduced 3PCF does not correlate with the stellar mass on small scales. On large scales, the shape dependence of the reduced 3PCF is stronger for lower-mass galaxies. The reduced 3PCF in the projected space shows weaker shape dependence but stronger stellar mass and color dependence, indicating that the redshift-space distortion reduces the dependence on galaxy properties. Red galaxies have higher amplitudes of the reduced 3PCF than those of the blue galaxies, implying that the nonlinear bias is important for the dependence on color.

Subject headings: galaxies: statistics , cosmology: observations , large-scale structure of Universe

1. INTRODUCTION

In the current paradigm of galaxy formation within a merging hierarchy of dark matter halos, galaxies form when gas is able to cool, condense and form stars at the centers of dark halos (White & Rees 1978). Galaxy formation thus involves complicated byronic processes that play crucial roles on galaxy and cluster scales but are poorly understood in many aspects. The situation is more complicated considering that the galaxy distribution is biased relative to the dark matter distribution and such biasing depends strongly on both spatial scale and galaxy properties (see e.g., Kaiser 1984; Bardeen et al. 1986). Studies of the galaxy distribution are expected to provide powerful constraints on models of galaxy formation and evolution.

It is common to use the two-point correlation function (2PCF) $\xi(r)$ to quantify the galaxy clustering in both theories and galaxy surveys (Davis & Geller 1976; Groth & Peebles 1977; Davis et al. 1985, 1988; Hamilton 1988; White et al. 1988; Boerner et al. 1989; Einasto 1991; Park et al. 1994; Loveday et al. 1995; Benoist et al. 1996; Guzzo et al. 1997; Beisbart & Kerscher 2000; Norberg et al. 2001; Zehavi et al. 2002, 2005, 2011; Li et al. 2006a, 2007; Skibba et al. 2006; Wang et al. 2007; Zheng et al. 2007; Swanson et al. 2008; Guo et al. 2013). The next order statistics in the hierarchy of N -point correlation functions, the three-point correlation function (3PCF)

$\zeta(r_1, r_2, r_3)$, is nevertheless not negligible. Because it is the lowest order to quantify the non-Gaussian features in the universe, which naturally arise in the nonlinear evolution of density fluctuation even in an initially Gaussian distributed density field (see e.g., Bernardeau et al. 2002). Although we generally assume a Gaussian primordial density field, which is completely described by the 2PCF, the 3PCF is also important when we want to characterize the primordial non-Gaussianity (Sefusatti & Komatsu 2007), e.g., in the cosmic microwave background (CMB) observations (Liguori et al. 2006, 2010; Komatsu et al. 2011).

Similar to the 2PCF, which measures the excess of galaxy pair counts over the random distribution, the 3PCF calculates the excess probability of triplets in the universe. So precise determination of the 3PCF requires a much larger galaxy sample. Meanwhile, since the number of triplets scales as N^3 , the measurement of the 3PCF is computationally more difficult. Consequently, while the dependence of the 2PCF on galaxy properties (such as luminosity, color and stellar mass) has been investigated extensively in literature (e.g., Zehavi et al. 2005, 2011; Li et al. 2006a; Meneux et al. 2008; Guo et al. 2013), the observational research on the similar dependence in 3PCF is still in slow progress. Many previous works using the observational data to measure the 3PCF or its Fourier-space counterpart, the bispectrum, put their focus on the constraints of galaxy biasing (Gaztanaga & Frieman 1994; Scoccimarro et al. 2001; Verde et al. 2002; Jing & Börner 2004; Gaztañaga et al. 2005; Nishimichi et al. 2007; Guo & Jing 2009a; McBride et al. 2011b).

Instead of directly studying the 3PCF, it is generally more convenient to define the reduced 3PCF, $Q(r_1, r_2, r_3)$, as the ratio between the 3PCF $\zeta(r_1, r_2, r_3)$ and the sum of the products of the 2PCFs. Such hierarchical scaling ($\zeta \propto \xi^2$) was introduced by Groth & Peebles (1977) assuming Q to be a constant.

¹ Partner Group of the Max Planck Institute for Astrophysics at the Shanghai Astronomical Observatory and Key Laboratory for Research in Galaxies and Cosmology of Chinese Academy of Sciences, Nandan Road 80, Shanghai 200030, China

² Department of Physics and Astronomy, University of Utah, 115 South 1400 East, Salt Lake City, UT 84112, USA

³ Center for Astronomy and Astrophysics, Physics Department, Shanghai Jiao Tong University, Shanghai 200240, China

⁴ Max-Planck-Institut für Astrophysik, Karl-Schwarzschild-Strasse 1, 85748 Garching, Germany

Although the following theories and observations found that Q is generally dependent on the size and shape of the triangle (r_1, r_2, r_3) (see e.g., [Bernardeau et al. 2002](#)), it is still more natural to use Q as the measurement of non-Gaussianity generated from gravitational clustering. The 3PCF itself is of less interest in view of hierarchical clustering as we can now precisely measure the 2PCF.

In observation, the redshift-space distortion (RSD) effect will significantly change the shape and amplitude of both 2PCF and 3PCF, because galaxy peculiar velocities prevent us from measuring the real radial distribution of the galaxies. On small scales, the RSD will make the galaxy distribution stretched along the line of sight, known as the ‘‘Fingers-of-God’’ effect ([Jackson 1972](#)). On large scales, the structures in redshift space will be squashed along the line of sight by the large-scale infall, which is often referred to as the Kaiser effect ([Kaiser 1987](#)). Projected correlation function is then used to minimize the influence of the RSD and it can be easily converted to the real-space correlation function ([Davis et al. 1985](#)). So the projected 3-point correlation function was proposed to the 3PCF in the real-space. [Jing & Börner \(1998\)](#) applied this statistic to the Las Campanas galaxy redshift survey.

[Jing & Börner \(2004\)](#) used the Two-Degree Field Galaxy Redshift Survey (2dFGRS; [Colless et al. 2001](#)) to measure the luminosity dependence of Q both in redshift and projected spaces. They found a small but significant trend that more luminous galaxies have lower amplitudes of Q . [Gaztañaga et al. \(2005\)](#) also measured the redshift-space Q with 2dFGRS and found a weak tendency for Q to decrease with increasing luminosity in the nonlinear regime. [Kayo et al. \(2004\)](#) and [Nichol et al. \(2006\)](#) employed the early data release (EDR) of the Sloan Digital Sky Survey (SDSS; [York et al. 2000](#)) and found no significant dependence of Q on galaxy morphology, color, or luminosity. Considering the measurement errors, their results are statistically consistent with [Jing & Börner \(2004\)](#) and [Gaztañaga et al. \(2005\)](#). Apart from the analysis of the observational data, another way to study the RSD is using numerical simulations (e.g., [Gaztañaga & Scoccimarro 2005](#); [Marín et al. 2008](#)). [Marín et al. \(2008\)](#) used N -body simulations to construct mock galaxy catalogs and compared Q in real and redshift spaces. They also found the same luminosity dependence of Q as in the observation and they argued that the color dependence of Q appears stronger than the luminosity dependence, which is consistent with the finding of [Gaztañaga et al. \(2005\)](#).

Recently, [McBride et al. \(2011a\)](#) explored the dependence of Q on luminosity and color in redshift and projected spaces using SDSS DR6. They measured the reduced 3PCF at $3\text{--}27 h^{-1}\text{Mpc}$ and compared the luminosity dependence for galaxies of r -band absolute magnitude $M_r < -19.5$. They found similar luminosity and color dependence to the previous works and inferred that the weak configuration dependence of Q on small scales is caused by the RSD. They also used these measurements to infer the galaxy bias and found the linear bias model to better agree with the current constraints on σ_8 ([McBride et al. 2011b](#)).

In this paper, we will use the final release data (DR7; [Abazajian et al. 2009](#)) of SDSS to measure the 3PCF in both redshift and projected spaces following the work

of [Jing & Börner \(2004\)](#). Different to the previous results, we will investigate the luminosity, color as well as the stellar mass dependence, considering the importance of stellar mass as a more physical parameter of galaxies ([Li et al. 2006a](#); [Li & White 2009](#)). Since the stellar mass dependence of the 3PCF has never been studied before, it will provide more constraints on the current galaxy formation models. We extend the previous analysis by exploring galaxy samples to a broader range of luminosity and scales and we investigate more triangle configurations to identify whether the weak configuration dependence of Q is really caused by the RSD.

The paper is constructed as follows. In Section 2, we briefly describe the galaxy and mock samples. The methods of measuring the 2PCF and 3PCF are presented in Section 3. We present our results of the stellar mass, luminosity and color dependence of the 3PCF in Section 4. We summarize our results in Section 5.

Throughout this paper we assume a cosmology model with the density parameter $\Omega_m = 0.3$ and the cosmological constant $\Omega_\Lambda = 0.7$, and a Hubble constant $H_0 = 100 h \text{kms}^{-1} \text{Mpc}^{-1}$ with $h = 1.0$.

2. DATA

2.1. SDSS galaxy samples

The galaxy sample used in this paper is a magnitude-limited sample taken from the New York University Value-Added Galaxy Catalog (NYU-VAGC), constructed by [Blanton et al. \(2005\)](#) based on SDSS DR7. This sample has formed the basis for the recent studies on the galaxy distribution in the low-redshift universe (e.g., [Li et al. 2012a,b, 2013](#)). The sample contains about half a million galaxies located in the main contiguous area of the survey in the Northern Galactic Cap, with $r < 17.6$, $-24 < M_r < -16$, and spectroscopically measured redshifts in the range of $0.001 < z < 0.5$. Here r is the r -band Petrosian apparent magnitude, corrected for Galactic extinction, and M_r is the r -band Petrosian absolute magnitude, corrected for evolution and K -corrected to $z = 0.1$. The apparent magnitude limit is chosen to select a sample that is uniform and complete over the entire area of the survey (see [Tegmark et al. 2004](#)). The median redshift of this sample is $z = 0.088$, with 10% of the galaxies below $z=0.033$ and 10% above $z=0.16$.

The stellar mass of each galaxy in our sample accompanies the NYU-VAGC release. It is estimated based on the redshift and the five-band Petrosian magnitudes from SDSS photometric data, as described in detail in [Blanton & Roweis \(2007\)](#). This estimate corrects implicitly for dust and assumes a universal stellar initial mass function (IMF) of [Chabrier \(2003\)](#) form. As demonstrated in Appendix A of [Li & White \(2009\)](#), once all estimates are adapted to assume the same IMF, the estimated stellar masses agree quite well with those obtained from the simple, single-color estimator of [Bell et al. \(2003\)](#) and also with those derived by [Kauffmann et al. \(2003\)](#) from a combination of SDSS photometry and spectroscopy.

From this sample we select two sets of samples according to either r -band absolute magnitude (M_r) or stellar mass ($\log_{10} M_s$). In each of these samples, we further divide the galaxies into *red* and *blue* populations according their $g - r$ color, following the luminosity-dependent

color divider determined in Li et al. (2006a). Details of the luminosity-/mass-selected samples, as well as their red/blue samples, are listed in Table 1.

2.2. Random samples

To obtain reliable estimates of the auto-correlation functions, each observed sample in Table 1 must be compared with a “random sample” which is unclustered but fills the same region of the sky and has the same, position-dependent spectroscopic completeness and luminosity-dependent redshift distribution. We construct our random samples from the observed samples themselves, as described in detail in Li et al. (2006a). For each real galaxy we generate 10 sky positions at random within the mask of the survey (see Blanton et al. 2005, for details), and we assign to each of them the properties of the real galaxy, in particular, its values of redshift, luminosity and stellar mass, as well as the position-dependent spectroscopic completeness. Extensive tests show that random samples constructed in this way produce indistinguishable results from those using the traditional method (Li et al. 2006b).

2.3. Mock galaxy samples

We construct a set of 80 mock SDSS galaxy catalogs from the Millennium Simulation (Springel et al. 2005) using both the sky mask and the magnitude and redshift limits of our real SDSS sample. The Millennium Simulation uses 10^{10} particles to follow the dark matter distribution in a cubic region with $500h^{-1}\text{Mpc}$ on a side, assuming the concordance Λ cold dark matter cosmology. Galaxy formation within the evolving dark matter halos is simulated in postprocessing using semi-analytic methods tuned to give a good representation of the observed low-redshift galaxy population. Our mock catalogs are based on the galaxy formation model of Croton et al. (2006) and are constructed from the publicly available data at $z = 0$ using the methodology of Li et al. (2006b) and Li et al. (2007). These mock catalogs allow us to derive realistic error estimates for the correlation functions we measure, including both sampling and cosmic variance uncertainties. We use all the 80 mock catalogs for estimating the errors of our two-point correlation function measurements. For the three-point correlation functions, we use 10 mock catalogs randomly selected from the whole set, in order to save computational time while obtaining reasonably good estimation of errors.

3. CORRELATION FUNCTION MEASUREMENTS

3.1. Two-point Correlation Function

We begin by estimating the two-dimensional, redshift-space, two-point auto-correlation function for each of the samples listed in Table 1, $\xi(r_p, r_\pi)$, using the estimator of Landy & Szalay (1993):

$$\xi(r_p, r_\pi) = \frac{\text{DD} - 2\text{DR} + \text{RR}}{\text{RR}}, \quad (1)$$

where DD, DR and RR are the data-data, data-random and random-random pair counts, and r_p and r_π are the pair separations perpendicular and parallel to the line of sight. To normalize appropriately, RR needs to be multiplied by $(N_g/N_r)^2$ and DR by N_g/N_r where N_g and N_r are the numbers of galaxies in the real and random

samples, respectively. In our case, $N_r = 10 \times N_g$. We have corrected the effect of fiber collisions in the same way as in Li et al. (2006b) and Li et al. (2007). Detailed tests of the method can be found in Li et al. (2006b) and Guo et al. (2012).

Next, we integrate these two-dimensional correlation estimates over the line-of-sight separation r_π to obtain the projected auto-correlation function, $w_p(r_p)$, as follows,

$$w_p(r_p) = \int_{-r_{\pi, \max}}^{+r_{\pi, \max}} \xi(r_p, r_\pi) dr_\pi = \sum_i \xi(r_p, r_\pi) \Delta r_{\pi, i}, \quad (2)$$

where we choose $r_{\pi, \max} = 40h^{-1}\text{Mpc}$ as the outer limit for the integration depth (in order to reduce the noise from distant uncorrelated regions) so that the summation for computing $w_p(r_p)$ runs from $r_{\pi, 1} = -39.5h^{-1}\text{Mpc}$ to $r_{\pi, 80} = 39.5h^{-1}\text{Mpc}$, given that we use bins of width $\Delta r_{\pi, i} = 1h^{-1}\text{Mpc}$.

In addition to $w_p(r_p)$, we also measure the one-dimensional auto-correlation function in redshift space, $\xi(s)$, using the same estimator in Equation (1) but as a function of s , the redshift-space three-dimensional pair separation, which is given by

$$s = \sqrt{r_p^2 + r_\pi^2}. \quad (3)$$

The measurements of $w_p(r_p)$ and $\xi(s)$ for the four luminosity-selected samples are presented in Figure 1. For clarity, we show the $w_p(r_p)$ errors only for the luminosity sample of $-20 < M_r < -19$, which are estimated from the 80 mock catalogs as described in the previous section. In all cases, both $w_p(r_p)$ and $\xi(s)$ show systematic trends with luminosity, reflecting the well known fact that more luminous galaxies are clustered more strongly. The projected two-point correlation function can be separated into two parts: a steeper inner part at pair separations below $\sim 1h^{-1}\text{Mpc}$ and a flatter outer part at larger separations. In the language of “halo model” (Cooray & Sheth 2002), the inner part is called *one-halo* term where the pair counts are mostly galaxy pairs in the same halo, and the outer part is called *two-halo* term where galaxy pairs are mostly from separate halos. The separation where the transition between the two terms occurs increases with increasing luminosity. In the two-halo term, the amplitude of $w_p(r_p)$ is an increasing function of luminosity, while its slope shows weak or no luminosity dependence. This is consistent with the picture that, on large scales, the bias in the galaxy distribution is related in a simple way to the bias in the distribution of dark halos. In contrast, the one-halo term is a strong increasing function of galaxy luminosity, in both amplitude and slope (see also, Zehavi et al. 2011). This indicates that galaxies of different luminosities are distributed within their host halos in different ways. When compared to the projected correlation function, the $\xi(s)$ measurements are relatively suppressed on small scales, leading to almost no transition between the one-halo and two-halo terms. This is caused by the redshift distortion effect on small scales and the global infall towards high-density regions on large scales.

Both the projected and redshift-space two-point correlation functions have been extensively studied in

TABLE 1
FLUX-LIMITED SAMPLES OF DIFFERENT LUMINOSITY AND STELLAR MASS

Sample	M_r	Number of galaxies	Red Galaxies	Blue Galaxies
L1	[-19,-18)	36223	13127	23096
L2	[-20,-19)	107241	52169	55072
L3	[-21,-20)	189880	102128	87752
L4	[-22,-21)	118728	73002	45726
Sample	$\log_{10}(M_s/h^2 M_\odot)$	Number of galaxies	Red Galaxies	Blue Galaxies
M1	[9.0,9.5)	32573	6658	25915
M2	[9.5,10)	84024	30700	53324
M3	[10,10.5)	181865	97918	83947
M4	[10.5,11)	143235	99932	43303

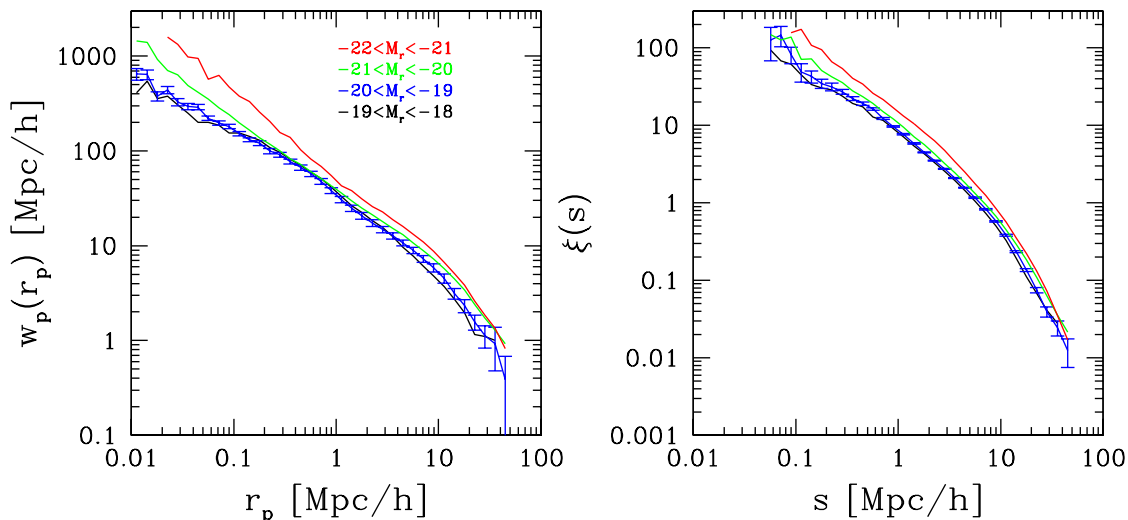


FIG. 1.— Projected- (left panel) and redshift-space (right panel) two-point correlation functions for different luminosity samples. Lines of different color denote different luminosity samples, with the black, blue, green, and red for $L1$, $L2$, $L3$, and $L4$ respectively. We only show the errors for one sample for clarity.

literature using both SDSS-based samples (see e.g., Zehavi et al. 2005, 2011; Li et al. 2006a; Guo et al. 2013) and samples from other surveys. Our measurements are well consistent with those previous determinations (more detailed comparisons will be presented in a separate paper by Li et al.). In the current paper, these two-point autocorrelation measurements for different stellar mass, color and luminosity bins will be used in what follows to determine the reduced three-point correlation functions.

3.2. Three-point Correlation Function

By analogy with the case of 2PCF, if we want to define the 3PCF in the projected space, we need five free parameters, $(r_{p12}, r_{p23}, r_{p31}, r_{\pi12}, r_{\pi23})$, where r_{pij} and $r_{\pi ij}$ are the separations of objects i and j perpendicular to and along the line of sight. The physical explanation of the 3PCF $\zeta(r_{p12}, r_{p23}, r_{p31}, r_{\pi12}, r_{\pi23})$ is the excess probability of finding three objects simultaneously in three volume elements dV_1 , dV_2 , and dV_3 at positions \mathbf{s}_1 , \mathbf{s}_2 and \mathbf{s}_3 , excluding the contributions from the 2PCFs,

$$dp_{123} = \bar{n}(\mathbf{s}_1)\bar{n}(\mathbf{s}_2)\bar{n}(\mathbf{s}_3) \times [1 + \xi(r_{p12}, r_{\pi12}) + \xi(r_{p23}, r_{\pi23}) + \xi(r_{p31}, r_{\pi31}) + \zeta(r_{p12}, r_{p23}, r_{p31}, r_{\pi12}, r_{\pi23})] dV_1 dV_2 dV_3. \quad (4)$$

The projected 3PCF $\Pi(r_{p12}, r_{p23}, r_{p31})$ and its reduced counterpart $Q_p(r_{p12}, r_{p23}, r_{p31})$ are defined as (Jing & Börner 1998, 2004)

$$\Pi(r_{p12}, r_{p23}, r_{p31}) = \int \zeta(r_{p12}, r_{p23}, r_{p31}, r_{\pi12}, r_{\pi23}) dr_{\pi12} dr_{\pi23} \quad (5)$$

$$Q_p(r_{p12}, r_{p23}, r_{p31}) = \frac{\Pi(r_{p12}, r_{p23}, r_{p31})}{w_p(r_{p12})w_p(r_{p23}) + \text{cyc}}. \quad (6)$$

Similarly, the redshift space reduced 3PCF is defined by,

$$Q_s(s_{12}, s_{23}, s_{31}) = \frac{\zeta(s_{12}, s_{23}, s_{31})}{\xi(s_{12})\xi(s_{23}) + \text{cyc}}. \quad (7)$$

We use the following estimator to measure ζ and Π in our samples (Szapudi & Szalay 1998),

$$\zeta = \frac{\text{DDD} - 3\text{DDR} + 3\text{DRR} - \text{RRR}}{\text{RRR}}, \quad (8)$$

where DDD, DDR, DRR and RRR are the normalized number counts of triplets in each bin measured from data (represented by D) and random samples (represented by R). We set the maximum of integration over the line of sight as $r_{\pi, \text{max}} = 40 h^{-1} \text{Mpc}$ for both $r_{\pi12}$ and $r_{\pi23}$. The binning of r_π is defined as $\Delta r_\pi = 1 h^{-1} \text{Mpc}$. The choice

of Δr_π is important for the projected 3PCF because it is more sensitive to the spacial structure (McBride et al. 2011a).

Instead of using (r_1, r_2, r_3) to represent the triangle, we use the parametrization of (r_1, r_2, θ) , with $r_2 \geq r_1$ and $\theta = \arccos[(r_1^2 + r_2^2 - r_3^2)/2r_1r_2]$. We note that in this parametrization, one triangle is counted three times in different bins of (r_1, r_2, θ) . But it does not affect our measurements of the configuration dependence, once we do not combine the counts in different bins together. Following Jing & Börner (2004), we use the same logarithmic binning for r_1 and r_2 , but linear binning for θ and π . The choice of $\Delta\theta$ is $\Delta\theta = \pi/20$, which is small enough to trace the dependence on θ . Unless a very large bin size (e.g., $\Delta\theta = \pi/5$) is used, decreasing the bin size of θ in our samples does not improve the results but only reduce the signal-to-noise ratio (S/N) (Marín 2011). Considering the importance of binning scheme for the measurements of the three-point correlation function (see e.g., Gaztañaga & Scoccimarro 2005; Kulkarni et al. 2007; Marín et al. 2008; McBride et al. 2011a), we investigate the influence of the binning in r_1 and r_2 on the reduced 3PCF in Figure 2. Without loss of generality, we present the results only for the galaxy sample of $-21 < M_r < -20$, which is the largest sample in luminosity. We require that $\bar{r}_2 \equiv 2\bar{r}_1$ and $\Delta \log r_2 = \Delta \log r_1$, where \bar{r}_1 and \bar{r}_2 are the mean in logarithmic space, i.e. the range of r_1 is $\log \bar{r}_1 - \Delta \log r_1/2 < \log r_1 < \log \bar{r}_1 + \Delta \log r_1/2$. Different lines in Figure 2 represent different $\Delta \log r_1$, with red, blue and black lines for $\Delta \log r_1 = 0.05, 0.15$ and 0.25 , respectively. We only show the errors for the blue lines for clarity. For this test, the errors are calculated from the bootstrap resampling method (Jing & Börner 2004).

We find that using larger bin sizes will generally reduce the amplitude of both Q_s and Q_p , which is caused by the strong scale dependence of Q . The different bin sizes do not significantly affect the shapes of Q_s and Q_p . It seems to contradict the conclusions from McBride et al. (2011a) and Marín (2011), who show that larger bins will smooth out the configuration dependence of Q . This is due to the fact that they measured the 3PCF in bins of r_1, r_2 and r_3 , with the bin-width $\Delta r_i \propto r_i$, i.e., logarithmic bins in r_1, r_2 and r_3 . The binning scheme of r_1 and r_2 is similar to ours, but we measure the 3PCF in bins of r_1, r_2 and θ , and employ linear binning for θ . Using logarithmic binning in r_3 leads to overlaps in neighboring bins of θ after the conversion from (r_1, r_2, r_3) to (r_1, r_2, θ) . Such overlapping changes the shape dependence of Q . Figure 2 shows that comparing the measurements of Q from different papers with different binning schemes does not make sense. In order to have a reasonable S/N, we use different $\Delta \log r_1$ on different scales, but the comparison of Q for galaxies with different properties are made under the same binning scheme.

Another commonly-used parametrization of Q is (r, u, θ) , where $r \equiv r_1$, $u \equiv r_2/r_1$ and θ is the angle between r_1 and r_2 (e.g., Scoccimarro et al. 2001; Kayo et al. 2004; Nichol et al. 2006; Kulkarni et al. 2007; Guo & Jing 2009b). The definition is similar to ours, except for the replacement of r_2 by u . Such parametrization is introduced to decompose the elements of the triangle into the scale (denoted by r) and shape (represented by

u and θ) components. We note that in this parametrization, $\Delta \log r_2 = \Delta \log r_1 + \Delta \log u$, which means that the bin-width of r_2 is always larger than that of r_1 . Including u complicates the analysis, because we also need to take into account the bin-width of u . In order to have a small enough bin-width, we would rather use r_2 instead of u and require that $\Delta \log r_2 = \Delta \log r_1$, which cannot be achieved with the parametrization of (r, u, θ) .

4. RESULTS

4.1. Stellar Mass Dependence

Without loss of generality, we show in Figure 3 the luminosity dependence of Q_s and Q_p for $\bar{r}_2/\bar{r}_1 = 2$ in order to compare with results of previous works. Lines of different color denote different luminosity samples, with the black, blue, green, and red lines for $L1, L2, L3$, and $L4$, respectively (from faint samples to luminous ones). There is strong dependence of Q on luminosity, with more luminous galaxies showing lower Q , consistent with the findings of Jing & Börner (2004), Gaztañaga et al. (2005) and McBride et al. (2011a).

We show in Figure 4 the stellar mass dependence of the redshift-space reduced 3PCF Q_s . Lines of different colors denote samples of different stellar mass, with the black, blue, green, and red for $M1, M2, M3$, and $M4$, respectively. We only show the errors for one sample for clarity. Different panels present the results of Q_s for different scales and shapes. Generally, there is a trend that more massive galaxies have a lower amplitude of Q_s . It is consistent with the finding that more luminous galaxies have a smaller Q_s (Jing & Börner 2004; McBride et al. 2011a), considering the strong correlation of stellar mass and luminosity. The two less massive samples, $M1$ and $M2$, have very similar amplitude of Q_s on all scales, except for the largest scale on the bottom right panel. It indicates that these two samples have similar spacial distribution on small scales.

A way to characterize the dependence of 3PCF on stellar mass is to compare the 3PCF itself, ζ , rather than the reduced value Q . We show in Figure 5 the stellar mass dependence of ζ for the case of $\bar{r}_2 = 2\bar{r}_1$. We find that more massive galaxies are clustered stronger than the less massive ones in the 3PCF, consistent with the results of 2PCF (Li et al. 2006a). Such stellar mass dependence of ζ is contrary to the stellar mass dependence of Q , because the stellar mass dependence of ξ^2 in Equation 7 is much stronger than that of the 3PCF. This can be understood from the larger galaxy bias of those more massive galaxies. In the second-order perturbation theory (see e.g., Bernardeau et al. 2002), the reduced 3PCF of the galaxies, Q_g , is related to that of the underlying dark matter, Q_m , through

$$Q_g = \frac{Q_m}{b_1} + \frac{b_2}{b_1^2}, \quad (9)$$

where b_1 and b_2 are the linear and non-linear bias factors. If we only consider the linear bias model, i.e. $b_2 = 0$, we find that a larger galaxy bias b_1 would produce a smaller Q_g . Although on small scales, the second-order perturbation theory fails because of the non-linear effects (Guo & Jing 2009b), and the galaxy bias factors become scale-dependent, it is still true that more massive galaxies would show larger differences between the clustering

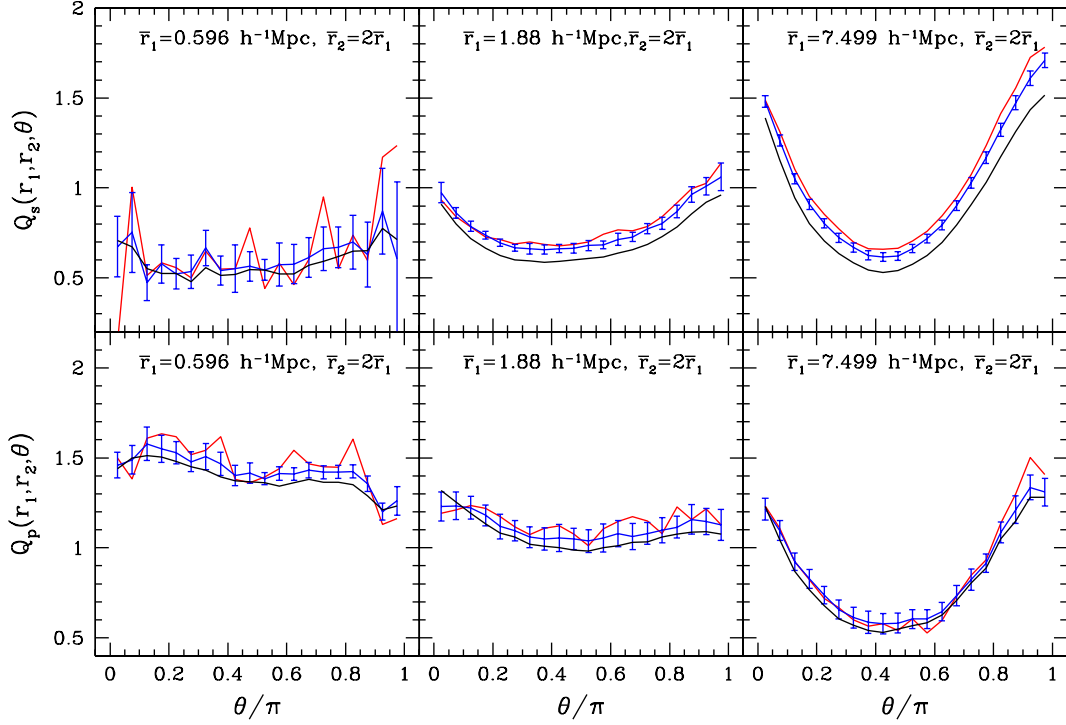


FIG. 2.— The influence of different $\Delta \log r_1$ bins for Q_s and Q_p . We present here the results of the galaxy sample with $-21 < M_r \leq -20$ and require $r_2 \equiv 2r_1$ and $\Delta \log r_2 = \Delta \log r_1$. The \bar{r}_1 and \bar{r}_2 values shown in the figure are the mean in logarithmic space, i.e. the range of r_1 is $\log \bar{r}_1 - \Delta \log r_1/2 < \log r_1 < \log \bar{r}_1 + \Delta \log r_1/2$. Different lines represent different $\Delta \log r_1$, with red, blue and black lines for $\Delta \log r_1 = 0.05, 0.15$ and 0.25 , respectively. We only show the errors for the blue lines for clarity. These errors are calculated from the bootstrap resampling method.

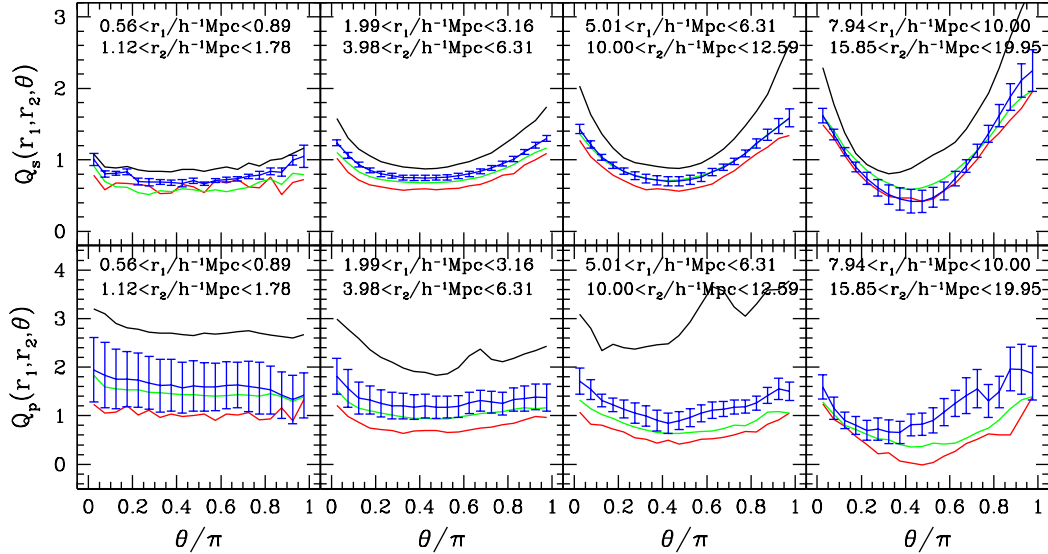


FIG. 3.— Reduced 3PCF in redshift (upper panels) and projected spaces (bottom panels) at different scales and triangle shapes. They are only shown for the case of $\bar{r}_2 = 2\bar{r}_1$. Lines of different colors denote different luminosity samples, with the black, blue, green, and red for $L1, L2, L3$, and $L4$, respectively. We only show the errors for one sample for clarity.

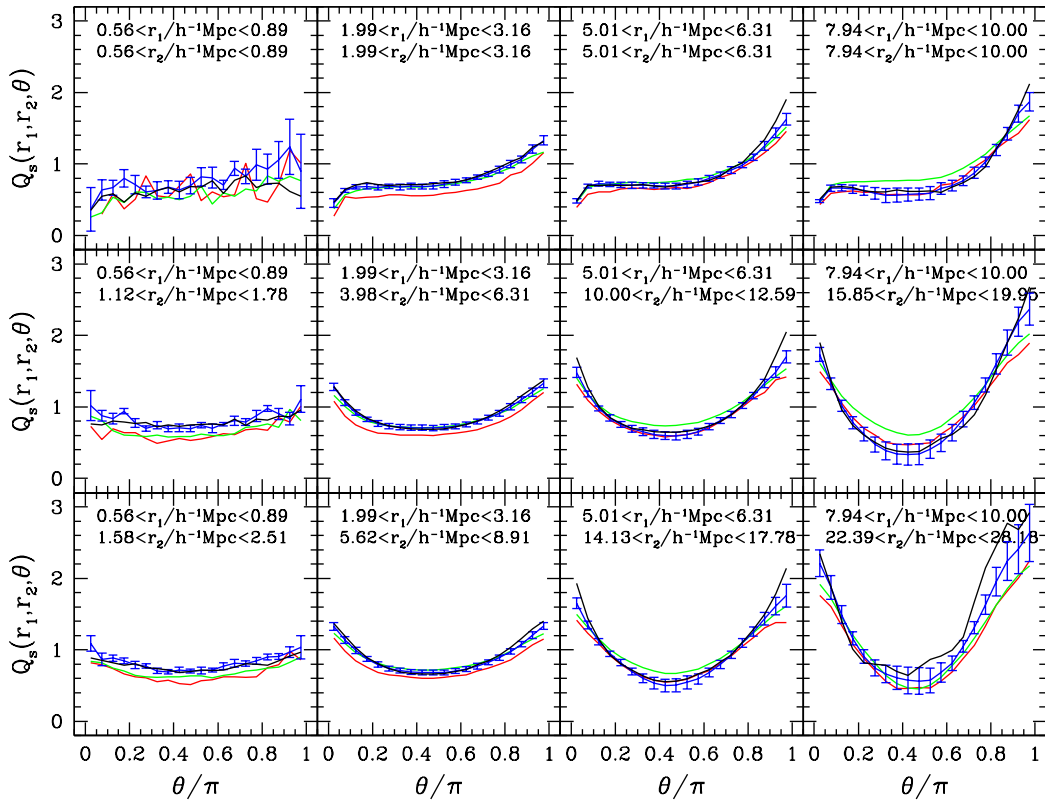


FIG. 4.— Redshift-space reduced 3PCF Q_s for different stellar mass samples at various scales and triangle shapes. Lines of different colors denote different stellar samples, with the black, blue, green, and red lines for M_1 , M_2 , M_3 , and M_4 respectively. We only show the errors for one sample for clarity.

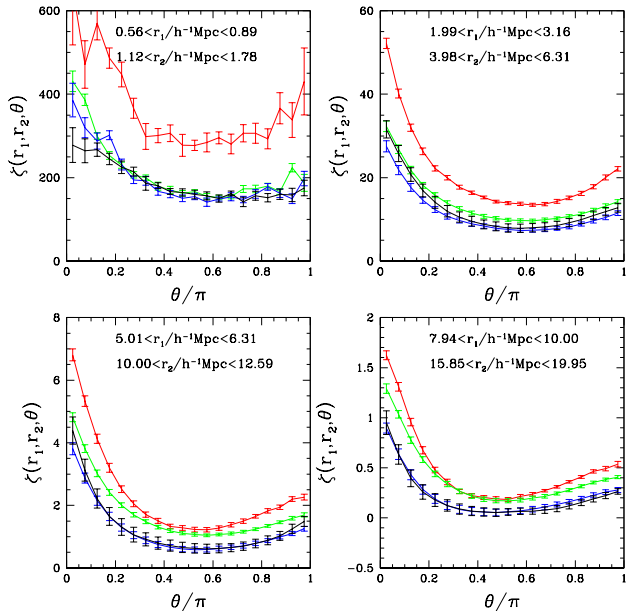


FIG. 5.— Three-point correlation function ζ for different stellar mass samples at various scales. The line styles are the same as in Figure 4. Only the case of $\bar{r}_2 = 2\bar{r}_1$ is shown.

strength of ξ^2 and ζ . In the linear bias model, we can express the galaxy 2PCF ξ_g as

$$\xi_g = b_1^2 \xi_m, \quad (10)$$

where ξ_m is the 2PCF of the dark matter. Therefore, we have $\zeta \sim Q_g \xi_g^2 \sim b_1^3 Q_m \xi_m^2$, confirming that ξ^2 varies much stronger ($\propto b_1^4$) with different stellar mass samples than ζ .

In the left panels of Figure 4, we find that Q is approaching a constant on small scales ($< 2 h^{-1} \text{Mpc}$), regardless of the stellar mass and shape. McBride et al. (2011a) measured Q on scales from $3 h^{-1} \text{Mpc}$ to $27 h^{-1} \text{Mpc}$, and found significant configuration dependence, which is not inconsistent with our results. In order to identify the correct scale of the triangle, we define the scale r_{max} as the maximum of (r_1, r_2, r_3) . Our measurements on these small scales ($< 2 h^{-1} \text{Mpc}$) show that the clustering hierarchy, $\zeta \propto \xi^2$, would be valid on scales of $r_{max} < 2 h^{-1} \text{Mpc}$. In principle, the clustering hierarchy implies that the higher-order N -point connected correlation functions can be determined by only using the 2PCF and a set of constant hierarchical amplitudes Q_N .

Comparing Figures 4 and 5, we find that while ζ decreases with the scale, the scale dependence of Q_s is two-sided. For elongated triangle shapes ($\theta \sim 0$, and π), Q_s increases with scale, while for the perpendicular triangles ($\theta \sim \pi/2$), there is a weak trend for Q_s to decrease as the scale increases. These two effects make Q_s show much stronger shape dependence on larger scales. On large scales, galaxies tend to be more clustered in linear structures, such as filaments (Scoccimarro et al. 2001). Less massive galaxies have stronger shape dependence and are thus more populated in these linear structures. Since galaxies of different stellar mass generally have different shapes of 2PCF (Li et al. 2006a), it

is indeed expected to find the degeneracy of the stellar mass and shape dependence on large scales.

The case $r_1 = r_2$ for Q_s is very special, because it shows a quite different configuration dependence as in other panels. With such triangles, the 3PCF can measure scales less than r_1 when $\theta < \pi/3$. The maximum scale (r_{max}) of the triangle is r_1 . It seems that the configuration dependence of Q_s shown in this way is determined by r_{max} of the triangle. If we define r_{max} as the scale, we can use the angle θ_{max} subtended by r_{max} as the configuration θ . Therefore, the mild shape dependence of Q_s seen in the top panels of Figure 4 when $\theta < \pi/3$ is caused by the fact that the θ_{max} subtended by r_{max} is only in the range of $[\pi/3, \pi/2]$ where the variation of Q_s with θ_{max} is small. So the shape dependence of Q_s is correlated with, but not determined by its scale dependence.

We present the stellar mass dependence for the projected-space reduced 3PCF Q_p in Figure 6. The result of the sample $M1$ is not shown in the bottom right panel, because these low-mass galaxies only cover a small volume and the large-scale measurements would suffer from the cosmic variance effect. The stellar mass dependence of Q_p is much stronger than that of Q_s . From Equation (9), it implies that the RSD would significantly affect our determination of the galaxy bias and its relation with the stellar mass, $b_1(M_s)$. We note that on small scales Q_p is also close to a constant, similar to that of Q_s .

In Figure 7, we compare Q_s and Q_p for the sample of $10.0 < \log(M_s) < 10.5$. We find that Q_p generally has weaker shape dependence than that of Q_s , different from the conclusion of McBride et al. (2011a), who show that the projected-space Q_p recovers more shape dependence that is lost to Q_s due to RSD. It is possible that the shape dependence shown in their figures is somewhat smoothed out by their choice of the parametrization (r_1, r_2, r_3) . Marín et al. (2008) compared the measurements of reduced 3PCF in real and redshift spaces for scales down to $r_1 = 1.5 h^{-1} \text{Mpc}$ using the N -body simulations. They found significant configuration dependence of Q in real space and concluded that the redshift-space distortions attenuate the shape dependence of Q . Since the projected correlation function is directly related to the real-space correlation function (Jing & Börner 2004), the weaker shape dependence of Q_p means that the real-space Q should also have weaker shape dependence. The projection effect does not change the shape dependence, but only accumulate the signals along the line-of-sight. On small scales, the virial motions of galaxies within the halos dominate the galaxy distribution, and the RSD would introduce more shape dependence. It is reasonable to infer that the RSD produces more shape dependence along the line of sight, while the projected Q_p would recover the correct signals at different directions.

4.2. Color Dependence

We show the color dependence of Q_s and Q_p for different stellar mass samples in Figures 8 and 9. The red and blue lines are for the red and blue galaxies defined in Section 2. The results for all the galaxies in the stellar mass samples are also shown as the black lines. We only display the results for the case of $\bar{r}_2/\bar{r}_1 = 2$. The differences between the 3PCFs of the red and blue galaxies are more apparent for less massive samples and on small

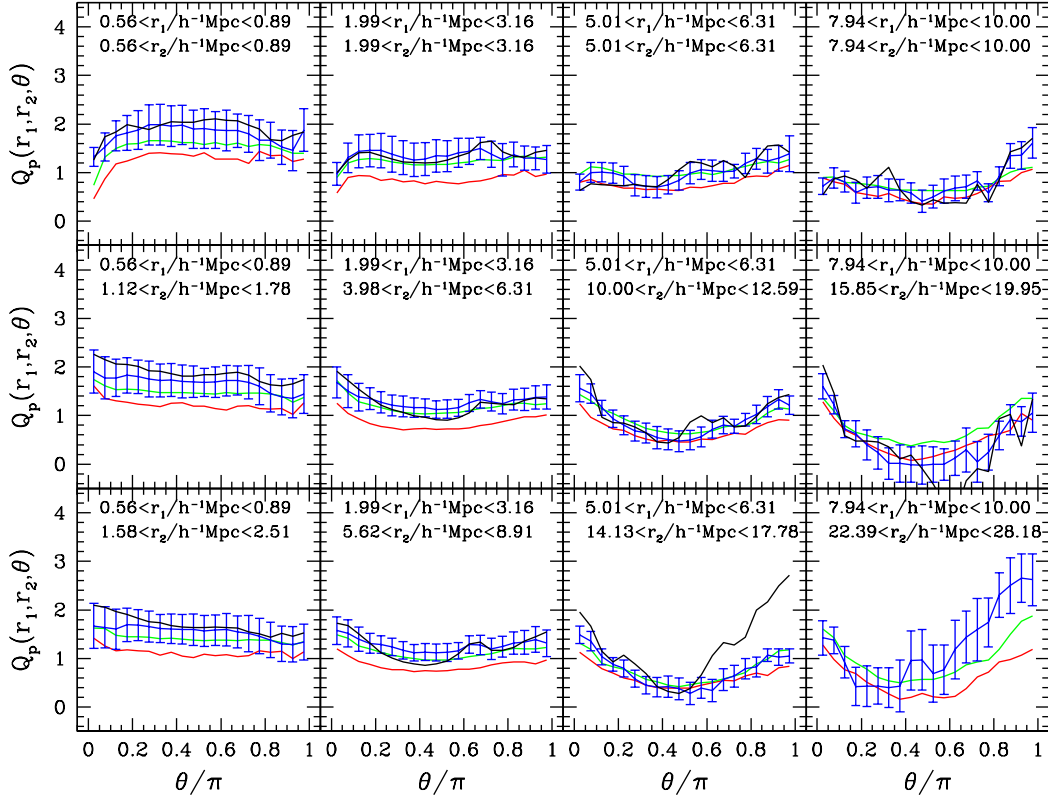


FIG. 6.— Same as in Figure 4, but for the projected-space reduced 3PCF Q_p .

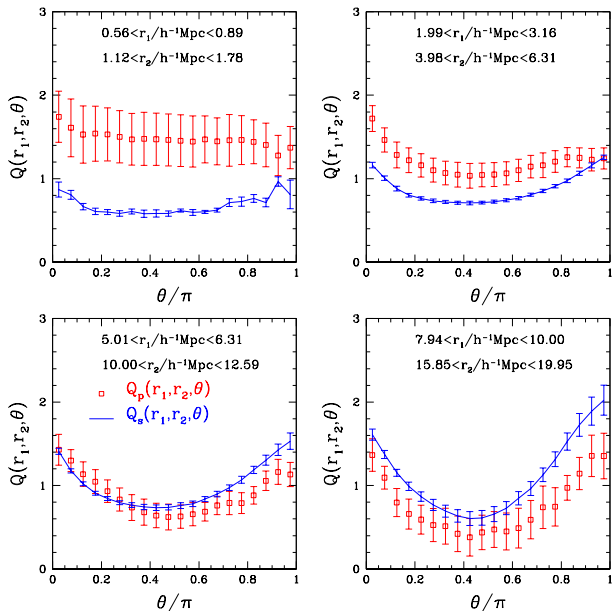


FIG. 7.— Comparison of the scale and shape dependence of Q_s (redshift space) and Q_p (projected space) for the stellar mass sample of $10.0 < \log(M_s) < 10.5$. The points are for Q_p and lines for Q_s .

scales. For the most massive galaxy sample in the right panels of Figures 8 and 9, there is only very weak dependence on color. Although in different stellar mass subsamples the fraction of red to blue galaxies varies a

lot, it only affects the shot noise levels of the measurements of different color samples and should not change the color dependence of Q .

Using high-resolution N -body simulations, Guo & Jing (2009b) demonstrate that the Equation (9) can be applied to measure the linear and nonlinear galaxy bias even on small scales where the second-order perturbation theory fails, although on small scales, the bias factors become scale-dependent. The red galaxies are found to have higher clustering amplitude than the blue galaxies in the 2PCF measurements (Zehavi et al. 2005; Li et al. 2006a), i.e. red galaxies have larger galaxy bias b_1 . For linear bias models, we expect Q for red galaxies to be smaller than that for blue galaxies, which is contrary to the results in Figures 8 and 9. This implies that the linear bias model is not enough to describe the galaxy bias of different color samples, in which case the nonlinear bias factor b_2 would not be negligible and plays an important role in Q . Considering that b_1 and Q are both larger for red galaxies, we infer from Equation (9) that the nonlinear bias b_2 of the red galaxies would also be larger than that of the blue ones.

In 2PCF, the differences between the clustering strength of the red and blue galaxies become smaller in more luminous galaxy samples and on larger scales (Li et al. 2006a). We also find a similar trend in Q . In the bottom panels of Figures 8 and 9, Q for the red and blue galaxies are more similar on large scales and in more massive galaxy samples, implying that the galaxy bias factors would have less dependence on color for these cases. We note that for low mass samples, red galaxies have stronger shape dependence than the blue galaxies,

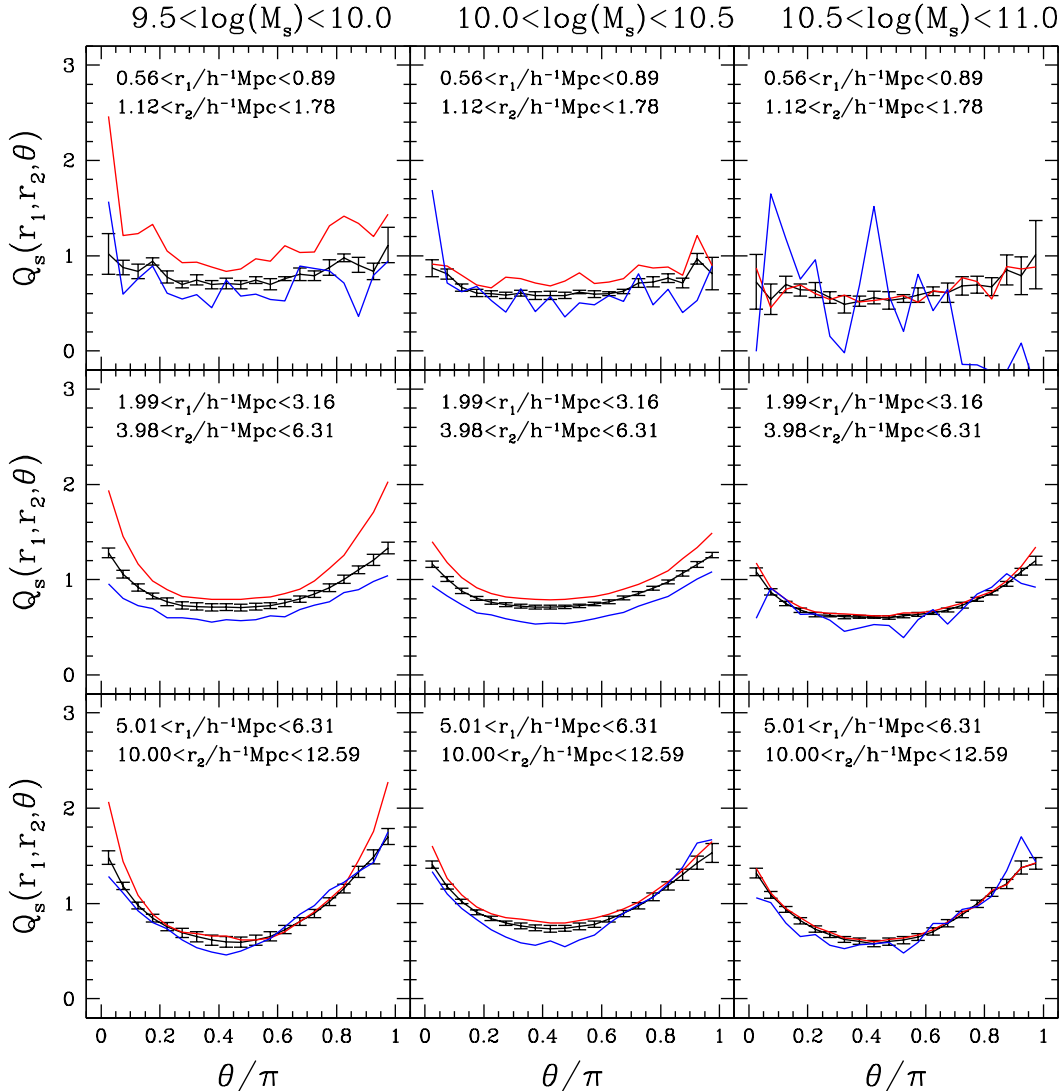


FIG. 8.— Redshift-space reduced 3PCF Q_s for different color samples at different stellar mass and scales. The red and blue solid lines are for red and blue galaxies defined in Section 2. The results for all the galaxies in the stellar mass samples are also shown as the black lines for comparison. We only display the results for $r_2/r_1 = 2$.

especially on large scales. This indicates that the low-mass red galaxies are more influenced by the large-scale structure and preferentially populate in the linear structures.

5. CONCLUSIONS AND DISCUSSIONS

In this paper, we measure stellar mass, color and luminosity dependence of the galaxy 3PCF using the SDSS DR7 main sample galaxies in the redshift range of $0.001 < z < 0.5$. We also investigate the scale and shape dependence of the 3PCF for samples of different stellar mass and color in both redshift and projected spaces.

There is a weak but significant dependence of the reduced 3PCF Q on galaxy stellar mass. More massive galaxies generally have higher amplitudes of the 3PCF ζ , but lower amplitudes of the reduced 3PCF Q , which is consistent with the finding that more luminous galaxies have smaller Q (Jing & Börner 2004; McBride et al. 2011a). Such behavior of the 3PCF is related to the

larger linear bias of more massive galaxies. The reduced 3PCF is also dependent on the scale and shape of the triangle, which provides a measurement of spacial directions in the galaxy distribution. We find that the shape dependence of Q is stronger on larger scales, reflecting the fact that the linear structures dominate the large-scale distribution. More massive galaxies show weaker shape dependence of Q , which is possibly resulting from the high occupancy of low-mass galaxies in the filamentary structures. The shape and scale dependence of Q is degenerate on large scales, and such degeneracy is not caused by the redshift distortion. The reduced 3PCF Q_s in redshift space and Q_p in projected space only have mild shape dependence on small scales ($< 2 h^{-1} \text{Mpc}$), regardless of stellar mass.

We investigate the color dependence of Q for different stellar mass samples. The color dependence is stronger for low-mass galaxies and on small scales, reflecting the different distribution of red and blue galaxies in the

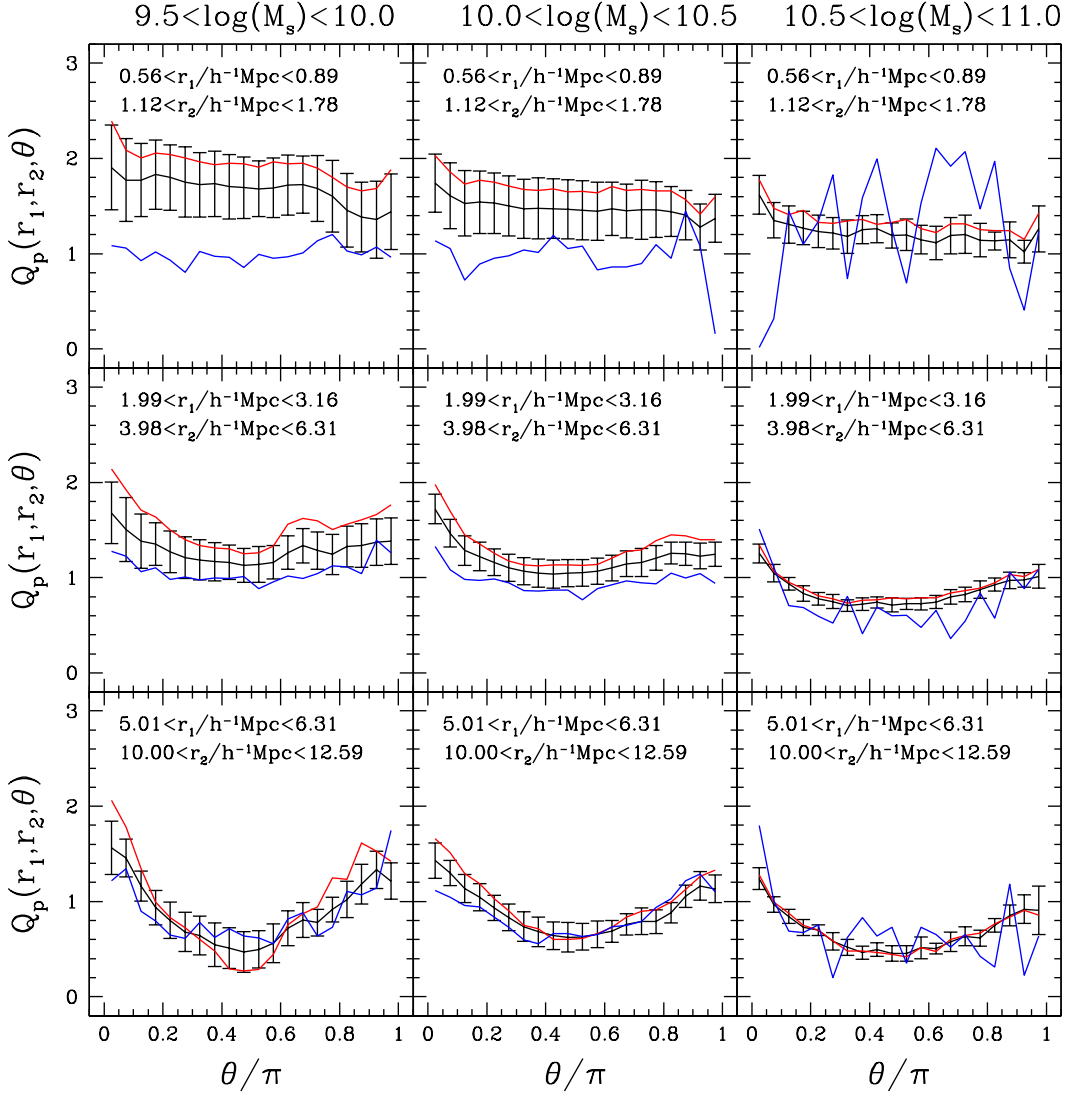


FIG. 9.— Same as in Figure 8, but for the projected-space reduced 3PCF Q_p .

small-scale structures. The red galaxies have higher clustering amplitudes and also higher Q values, which indicates that the linear bias models are not enough to describe the 3PCF distribution in comparison of various color samples. The nonlinear bias will be of importance for Q in the color distribution. The red galaxies display stronger shape dependence than blue galaxies in the low-mass samples and on large scales, which means that the red galaxies are more affected by the large-scale structures.

We use the projected reduced 3PCF to study the effect of redshift-space distortion in the dependence on stellar mass and color. We find that the redshift-space distortion would reduce the dependence on the galaxy properties. Since the projected-space Q_p shows weaker shape dependence than the redshift-space Q_s , we conclude that the redshift-space distortion will increase the shape dependence of Q . On large scales, the redshift distortion will have minimal effects on Q , so Q_s and Q_p converge on large scales. But the large-scale structure also signif-

icantly affect the measurement of the 3PCF. The measured Q_p suffers from larger shot noise fluctuation than Q_s .

These measurements of the three-point correlation function can be compared with the dark matter simulations to constrain galaxy bias, and they can also be used to constrain the galaxy formation and evolution models in the mock galaxy samples, which will be explored in future work.

This work is supported by NSFC (no. 11173045, no. 11233005) and the CAS/SAFEA International Partnership Program for Creative Research Teams (KJCX2-YW-T23). CL acknowledges the support of the 100 Talents Program of Chinese Academy of Sciences (CAS), Shanghai Pujiang Program (no. 11PJ1411600) and the exchange program between Max Planck Society and CAS.

Funding for the SDSS and SDSS-II has been provided by the Alfred P. Sloan Foundation, the Participating

Institutions, the National Science Foundation, the U.S. Department of Energy, the National Aeronautics and Space Administration, the Japanese Monbukagakusho, the Max Planck Society, and the Higher Education Funding Council for England. The SDSS Web Site is <http://www.sdss.org/>.

The SDSS is managed by the Astrophysical Research Consortium for the Participating Institutions. The Participating Institutions are the American Museum of Natural History, Astrophysical Institute Potsdam, University of Basel, University of Cambridge, Case Western Reserve University, University of Chicago,

Drexel University, Fermilab, the Institute for Advanced Study, the Japan Participation Group, Johns Hopkins University, the Joint Institute for Nuclear Astrophysics, the Kavli Institute for Particle Astrophysics and Cosmology, the Korean Scientist Group, the Chinese Academy of Sciences (LAMOST), Los Alamos National Laboratory, the Max-Planck-Institute for Astronomy (MPIA), the Max-Planck-Institute for Astrophysics (MPA), New Mexico State University, Ohio State University, University of Pittsburgh, University of Portsmouth, Princeton University, the United States Naval Observatory, and the University of Washington.

REFERENCES

- Abazajian, K. N., Adelman-McCarthy, J. K., Agüeros, M. A., et al. 2009, *ApJS*, 182, 543
- Bardeen, J. M., Bond, J. R., Kaiser, N., & Szalay, A. S. 1986, *ApJ*, 304, 15
- Beisbart, C., & Kerscher, M. 2000, *ApJ*, 545, 6
- Bell, E. F., McIntosh, D. H., Katz, N., & Weinberg, M. D. 2003, *ApJS*, 149, 289
- Benoist, C., Maurogordato, S., da Costa, L. N., Cappi, A., & Schaeffer, R. 1996, *ApJ*, 472, 452
- Bernardeau, F., Colombi, S., Gaztañaga, E., & Scoccimarro, R. 2002, *Phys. Rep.*, 367, 1
- Blanton, M. R., & Roweis, S. 2007, *AJ*, 133, 734
- Blanton, M. R., Schlegel, D. J., Strauss, M. A., et al. 2005, *AJ*, 129, 2562
- Boerner, G., Mo, H., & Zhou, Y. 1989, *A&A*, 221, 191
- Chabrier, G. 2003, *PASP*, 115, 763
- Colless, M., Dalton, G., Maddox, S., et al. 2001, *MNRAS*, 328, 1039
- Cooray, A., & Sheth, R. 2002, *Phys. Rep.*, 372, 1
- Croton, D. J., Springel, V., White, S. D. M., et al. 2006, *MNRAS*, 365, 11
- Davis, M., Efstathiou, G., Frenk, C. S., & White, S. D. M. 1985, *ApJ*, 292, 371
- Davis, M., & Geller, M. J. 1976, *ApJ*, 208, 13
- Davis, M., Meiksin, A., Strauss, M. A., da Costa, L. N., & Yahil, A. 1988, *ApJ*, 333, L9
- Einasto, M. 1991, *MNRAS*, 252, 261
- Gaztañaga, E., Norberg, P., Baugh, C. M., & Croton, D. J. 2005, *MNRAS*, 364, 620
- Gaztañaga, E., & Scoccimarro, R. 2005, *MNRAS*, 361, 824
- Gaztanaga, E., & Frieman, J. A. 1994, *ApJ*, 437, L13
- Groth, E. J., & Peebles, P. J. E. 1977, *ApJ*, 217, 385
- Guo, H., & Jing, Y. P. 2009a, *ApJ*, 698, 479
- . 2009b, *ApJ*, 702, 425
- Guo, H., Zehavi, I., & Zheng, Z. 2012, *ApJ*, 756, 127
- Guo, H., Zehavi, I., Zheng, Z., et al. 2013, *ArXiv e-prints*
- Guzzo, L., Strauss, M. A., Fisher, K. B., Giovanelli, R., & Haynes, M. P. 1997, *ApJ*, 489, 37
- Hamilton, A. J. S. 1988, *ApJ*, 331, L59
- Jackson, J. C. 1972, *MNRAS*, 156, 1P
- Jing, Y. P., & Börner, G. 1998, *ApJ*, 503, 37
- . 2004, *ApJ*, 607, 140
- Kaiser, N. 1984, *ApJ*, 284, L9
- . 1987, *MNRAS*, 227, 1
- Kauffmann, G., Heckman, T. M., White, S. D. M., et al. 2003, *MNRAS*, 341, 54
- Kayo, I., Suto, Y., Nichol, R. C., et al. 2004, *PASJ*, 56, 415
- Komatsu, E., Smith, K. M., Dunkley, J., et al. 2011, *ApJS*, 192, 18
- Kulkarni, G. V., Nichol, R. C., Sheth, R. K., et al. 2007, *MNRAS*, 378, 1196
- Landy, S. D., & Szalay, A. S. 1993, *ApJ*, 412, 64
- Li, C., Jing, Y. P., Kauffmann, G., et al. 2007, *MNRAS*, 376, 984
- Li, C., Kauffmann, G., Fu, J., et al. 2012a, *MNRAS*, 424, 1471
- Li, C., Kauffmann, G., Jing, Y. P., et al. 2006a, *MNRAS*, 368, 21
- Li, C., Kauffmann, G., Wang, L., et al. 2006b, *MNRAS*, 373, 457
- Li, C., Wang, L., & Jing, Y. P. 2013, *ApJ*, 762, L7
- Li, C., & White, S. D. M. 2009, *MNRAS*, 398, 2177
- Li, C., White, S. D. M., Chen, Y., et al. 2012b, *MNRAS*, 419, 1557
- Liguori, M., Hansen, F. K., Komatsu, E., Matarrese, S., & Riotto, A. 2006, *Phys. Rev. D*, 73, 043505
- Liguori, M., Sefusatti, E., Fergusson, J. R., & Shellard, E. P. S. 2010, *Advances in Astronomy*, 2010
- Loveday, J., Maddox, S. J., Efstathiou, G., & Peterson, B. A. 1995, *ApJ*, 442, 457
- Marín, F. 2011, *ApJ*, 737, 97
- Marín, F. A., Wechsler, R. H., Frieman, J. A., & Nichol, R. C. 2008, *ApJ*, 672, 849
- McBride, C. K., Connolly, A. J., Gardner, J. P., et al. 2011a, *ApJ*, 726, 13
- . 2011b, *ApJ*, 739, 85
- Meneux, B., Guzzo, L., Garilli, B., et al. 2008, *A&A*, 478, 299
- Nichol, R. C., Sheth, R. K., Suto, Y., et al. 2006, *MNRAS*, 368, 1507
- Nishimichi, T., Kayo, I., Hikage, C., et al. 2007, *PASJ*, 59, 93
- Norberg, P., Baugh, C. M., Hawkins, E., et al. 2001, *MNRAS*, 328, 64
- Park, C., Vogeley, M. S., Geller, M. J., & Huchra, J. P. 1994, *ApJ*, 431, 569
- Scoccimarro, R., Sheth, R. K., Hui, L., & Jain, B. 2001, *ApJ*, 546, 20
- Sefusatti, E., & Komatsu, E. 2007, *Phys. Rev. D*, 76, 083004
- Skibba, R., Sheth, R. K., Connolly, A. J., & Scranton, R. 2006, *MNRAS*, 369, 68
- Springel, V., White, S. D. M., Jenkins, A., et al. 2005, *Nature*, 435, 629
- Swanson, M. E. C., Tegmark, M., Blanton, M., & Zehavi, I. 2008, *MNRAS*, 385, 1635
- Szapudi, S., & Szalay, A. S. 1998, *ApJ*, 494, L41
- Tegmark, M., Blanton, M. R., Strauss, M. A., et al. 2004, *ApJ*, 606, 702
- Verde, L., Heavens, A. F., Percival, W. J., et al. 2002, *MNRAS*, 335, 432
- Wang, Y., Yang, X., Mo, H. J., & van den Bosch, F. C. 2007, *ApJ*, 664, 608
- White, S. D. M., & Rees, M. J. 1978, *MNRAS*, 183, 341
- White, S. D. M., Tully, R. B., & Davis, M. 1988, *ApJ*, 333, L45
- York, D. G., Adelman, J., Anderson, Jr., J. E., et al. 2000, *AJ*, 120, 1579
- Zehavi, I., Blanton, M. R., Frieman, J. A., et al. 2002, *ApJ*, 571, 172
- Zehavi, I., Zheng, Z., Weinberg, D. H., et al. 2005, *ApJ*, 630, 1
- . 2011, *ApJ*, 736, 59
- Zheng, Z., Coil, A. L., & Zehavi, I. 2007, *ApJ*, 667, 760